

Observed and Predicted Vertical Suspended Sediment Concentration Profiles and Bedforms in Oscillatory-Only Flow

J.J. Williams[†], P.S. Bell[†], P.D. Thorne[†], K. Trouw[‡], P.J. Hardcastle[†], and J.D. Humphery[†]

[†]Centre for Coastal and Marine Sciences
Proudman Oceanographic Laboratory
Bidston Observatory
Bidston Hill
Prenton, CH43 7RA, U.K.

[‡]Laboratorium voor Hydraulica
Burgerlijke Bouwkunde
KU Leuven
De Croylaan 2
3001 Haverlee, Belgium

ABSTRACT

WILLIAMS, J.J.; BELL, P.S.; THORNE, P.D.; TROUW, K.; HARDCASTLE, P.J., and HUMPHERY, J.D., 2000. Observed and predicted vertical suspended sediment concentration profiles and bedforms in oscillatory-only flow. *Journal of Coastal Research*, 16(3), 698-708. West Palm Beach (Florida), ISSN 0749-0208.

Measurements of hydrodynamic conditions and vertical suspended sediment concentration profiles, C-profiles, have been obtained above rippled sandy beds in a large wave flume. Measured values of wave height and period, water depth and sediment properties are used in well-known formulae to predict sediment dynamics and bed shear stresses due to waves. These data are then used in an existing convective model and a new model to predict C-profiles. Measured C-profiles and C-profiles predicted by the new model are shown to agree well for a range of grain sizes and wave conditions. Grain-scale bed roughness, defined using data from the model, is found to vary with the wave mobility number. Values for the wave mixing coefficient derived using the new model are tested and are found to agree well with published values and with theory.

ADDITIONAL INDEX WORDS: *Deltaflume, pump-sampling, hydraulic roughness, diffusion, vortex, diffusivity, wave mixing, acoustic bed imaging.*



INTRODUCTION

In most marine situations sandy sediments are generally moved as bedload by tidal currents during part of the tidal cycle. During storms this situation can change dramatically when, under the action of large waves, bed sediments are resuspended in appreciable quantities and are transported in suspension by even the weakest of tidal currents. Given the pivotal role played by waves in the mobilisation and resuspension of bed sediments, the present paper tests a new expression to predict the vertical profile of suspended sediment concentration due to waves.

Two basic mechanisms are responsible for entrainment and vertical mixing of sediments by wave-induced flows: a) the formation of a vortex in the lee of each ripple when the flow reverses at each half-wave cycle results in convection of sediment away from the bed (this vortex is unwound rapidly and sediment diffuses outwards and/or settles back to the bed); and b) turbulence generated through interactions between grains comprising the bed and the wave-induced flow and between vortices and the surrounding fluid results in the vertical diffusion of the sediment.

In order to examine at approximately field-scale vertical time-averaged suspended sediment concentration profiles, C-

profiles, under waves, measurements of wave-induced flows and suspended sediments have been obtained in a large wave flume. Whilst this work has been undertaken primarily to evaluate the performance of the large multi-sensor instrument STABLE (WILLIAMS *et al.*, 1998a), work in the present paper focuses attention upon C-profiles and bedforms measured during the experiments.

Following a description of the instrumentation and the experiments, methods used to calculate various hydrodynamic and sedimentological parameters used in models to predict C-profiles are described. Predicted values of these parameters are compared with measured values. Measured C-profiles are then compared with C-profiles predicted by two models: the first uses an existing expression based upon a convective approach (NIELSEN, 1992); and the second uses a new diffusion-based expression developed by WILLIAMS *et al.* (1997b, 1998a). Parameterisation and performance of the models is considered.

EQUIPMENT AND METHODS

The Delft Hydraulics Laboratory Deltaflume is a large wave flume approximately 230 m long, 5 m wide and 7 m deep. The facility has a capacity to generate regular and irregular waves with a height up to 2 m, Figure 1a, thereby permitting the study of wave phenomenon at virtually field-scale. In the sections below the following co-ordinate system

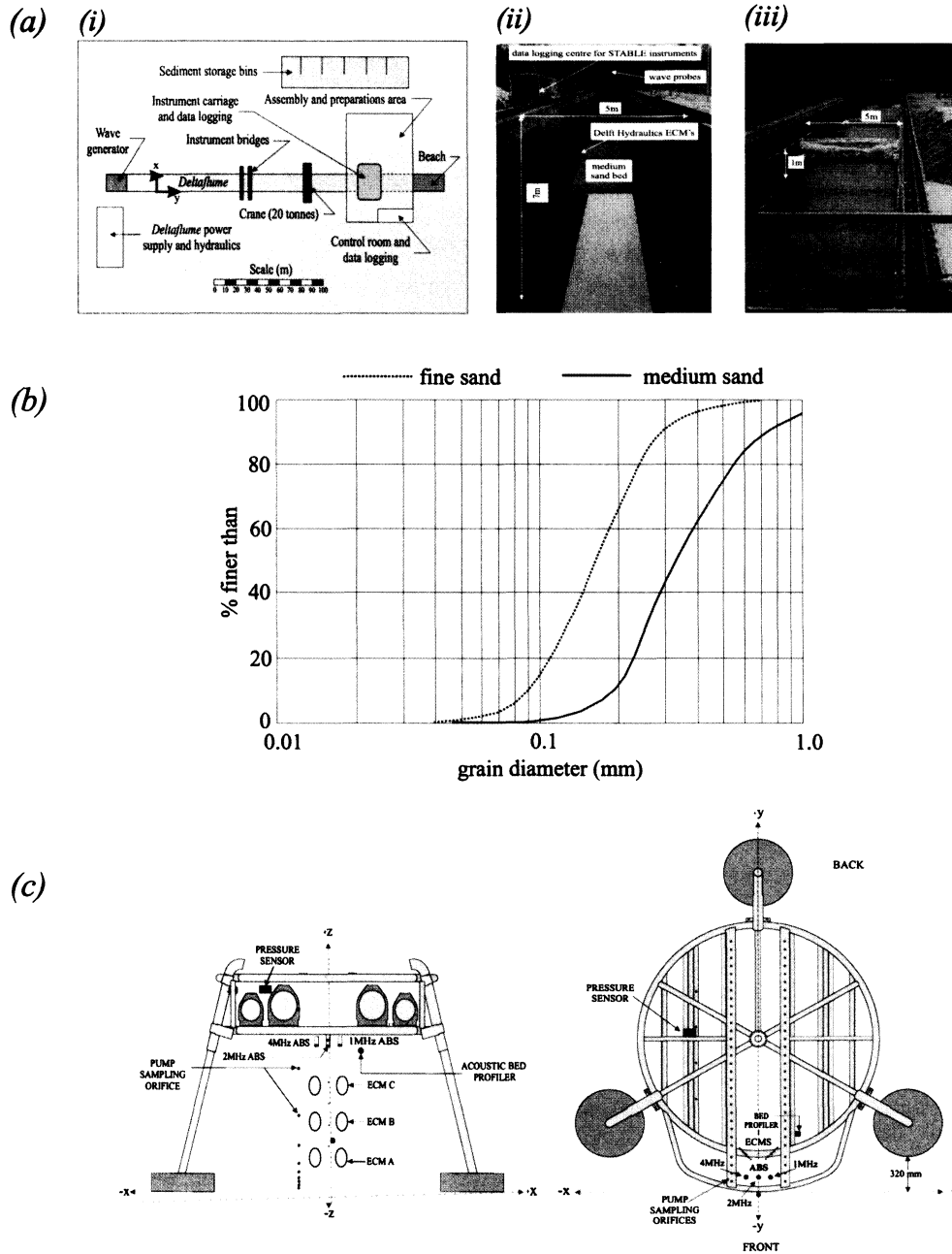


Figure 1. (a) Deltafume (b) grain size distribution (medium sand $D_{50} = 0.329$ mm; fine sand $D_{50} = 0.162$ mm) (c) STABLE - Sediment Transport And Boundary Layer Equipment.

is used to define the location of instruments: x = distance across the Deltafume; y = distance along the Deltafume from the wave generator; and z = the vertical distance above the sediment bed, Figure 1a(i).

Measurements were obtained above beds of sand comprising: (a) medium sand ($D_{10} = 0.187$ mm, $D_{16} = 0.211$ mm, $D_{35} = 0.273$ mm, $D_{50} = 0.329$ mm, $D_{84} = 0.605$ mm, $D_{90} = 0.761$ mm), test series A, Figure 1b; and (b) fine sand ($D_{10} = 0.093$ mm, $D_{16} = 0.101$ mm, $D_{35} = 0.135$ mm, $D_{50} = 0.162$ mm, D_{84}

$= 0.244$ mm, $D_{90} = 0.291$ mm), test series f, Figure 1b. The sandy beds, approximately 30 m long, 5 m wide and 0.5 m deep, Figure 1a(ii), were placed at $y = 105$ m, and were compacted by a mechanical vibrator. To reduce erosion, a slope of approximately 30° was left at each end of the sediment beds and drainage was laid beneath the beds to prevent disturbance to the sediments during filling of the Deltafume. Prior to taking any measurements, waves were passed over the test bed for approximately 5 hours in order to force re-

maining air out of the bed and to generate bedforms. Figure 1a(iii) shows 1.0 m regular waves in the Deltaflume during this initialisation.

Measurements of the water surface elevation were obtained at $y = 117.9$ m and $y = 120.9$ m using resistive wave probes. Data from these instruments were sampled at 25 Hz and were analysed subsequently using Delft Hydraulics software to calculate various wave parameters used in the sections below. Hydrodynamic and sediment measurements were obtained using a suite of sensors and sampling devices on the STABLE frame (HUMPHERY and MOORES, 1994; WILLIAMS *et al.*, 1997a), Figure 1c. Data used in the present study were obtained from STABLE using the following instruments: Valeport Series 800 electromagnetic current meters, ECM's (diameter = 10 cm, resolution = ± 0.1 cm/s); pump-sampling equipment; an acoustic bed profiler, ABP; and a sector scanning sonar, SSS. ECM's were used to measure wave-induced flow at a sampling rate of 8.0 Hz at $z \approx 30$ cm, 60 cm, and 91 cm.

Pump-sampling equipment used to obtain *in situ* samples of suspended sediment consisted of 10 brass intake nozzles (internal diameter 3 mm) orientated at 90° to the wave orbital motion (BOSMAN *et al.*, 1987; Figure 1c). Each nozzle in the array was connected to a plastic pipe through which a mixture of water and sediment was drawn to the surface by means of a peristaltic pump. The resulting water/sand mixture from each sampling position in the array was collected simultaneously in 10 litre buckets. Subsequent analysis of samples in the laboratory gave dry weight sediment concentration values and the suspended sediment grain size at each sampling height. During any given experiment, further samples of suspended sediment were obtained at 10 heights above the sand bed from the side-wall of the Deltaflume at $y = 121.5$ m using the same pump-sampling equipment.

The ABP (BELL and THORNE, 1997), measured the height, h_r , and wavelength, λ_r , of bedforms along a 3 m transect extending in front of and behind its location on the STABLE frame, Figure 1c. Completion of a single transect measurement took approximately 30 seconds and measurements were repeated immediately following the completion of the previous scan. With the wave generator turned off, acoustic images of the bed showing clearly wave-induced bedforms in a circular area of diameter ≈ 5.0 m were also obtained using a sector scanning sonar, SSS, device which was lowered into the Deltaflume (BELL *et al.*, 1998).

In order to minimise erosion of the bed, experimental conditions were chosen to run in sequence from low to high waves. Surveys showed that the depth of sediment either side of the STABLE deployment site remained approximately constant throughout the tests. The presence of equilibrium bedforms was assumed when the ABP failed to detect significant changes in h_r and λ_r . Normally this took approximately 60 minutes from the start of each new wave run. A summary of wave conditions pertaining during the experiments on the medium and fine sand beds considered here is given in Table 1. Irregular waves used in the experiments conformed to the JONSWAP spectrum.

Table 1. Approximate wave conditions for tests on the medium (A) and fine (f) sand beds (wave period ≈ 5 seconds in all cases).

Wave Height	Regular Waves		Irregular Waves	
	Medium Sand	Fine Sand	Medium Sand	Fine Sand
0.50	$\tau < \tau_c$	f03a	$\tau < \tau_c$	f04a
0.75	A08a	f11a	A09a	f07a
1.00	A05b	f08a	A10a	f10a
1.25	A11a		A12a	f12a

CALCULATION OF SEDIMENT AND HYDRAULIC PARAMETERS

During the experiments it was possible to measure most of the important sediment and hydrodynamic parameters used in published formulae to predict C-profiles. However, in most field situations, calculation of C-profiles must usually rely upon a very limited number of data (*e.g.*, wave height, wave period and the median grain size of the bed material) and usually recourse must be made, to empirical methods to predict other required parameters. Thus, before examining C-profiles in detail, here we calculate using well-known formulae, a number of important sediment and hydrodynamic parameters. These calculated values will be compared subsequently with measured values. In general, the choice of formulae used here follows guidance given by SOULSBY (1997).

Sediments

The median diameter of grains in suspension, D_{50S} , was calculated using

$$D_{50S} = D_{50}[1 + 0011(\sigma_s - 1)(T_s - 25)] \quad \text{for } 0 < T_s < 25 \quad (1)$$

and

$$D_{50S} = D_{50} \quad \text{for } T_s \geq 25, \quad (2)$$

VAN RIJN (1984), where the grain sorting parameter, $\sigma_s = 0.5 [(D_{84}/D_{50}) + (D_{50}/D_{16})]$ is based upon measured sediment properties, Figure 1b, and the sediment transport parameter, $T_s = (\hat{\tau}_{wG} - \tau_c)/\tau_c$. Methods used to calculate the peak skin-friction component of bed shear stress, $\hat{\tau}_{wG}$, and the threshold bed shear stress for sediment entrainment, τ_c , are described below.

The settling velocity of grains in suspension was calculated using the optimised formula

$$w_s = \frac{\nu}{D_{50S}} [(10.36^2 + 1.049D_{*S}^3)^{1/2} - 10.36] \quad (3)$$

SOULSBY (1997), where the dimensionless grain size for grains in suspension, D_{*S} , is given by

$$D_{*S} = \left[\frac{g \left(\frac{\rho_s}{\rho} - 1 \right)}{\nu^2} \right]^{1/3} D_{50S} \quad (4)$$

Here ν and ρ are the kinematic viscosity, ($\approx 1.11 \times 10^{-6}$ at 16° C), and the density, (≈ 999.0 kg/m³ at 16° C), of water, respectively, and ρ_s is the measured density of the sediment, (2653 kg/m³).

The threshold peak wave shear stress for bed sediment, τ_t , was calculated using

$$\tau_t = \theta_c g(\rho_s - \rho) D_{50} \quad (5)$$

where the critical Shields parameter (SOULSBY, 1997). In this case the dimensionless grain size, D_* , was calculated using $D_{50s} = D_{50}$ (Eq. 4).

Hydrodynamics

For monochromatic waves, the peak orbital velocity amplitude at the bed, \hat{U}_w , was calculated from linear theory using

$$\hat{U}_w = \frac{\pi H}{T \sinh(kh)} \quad (7)$$

where H is the measured wave height, T is the measured wave period, the wave number, $k = 2\pi/\lambda$, λ is the wavelength and h is the measured time-averaged water depth. For the irregular waves, \hat{U}_w was approximated from measured values of the significant wave height H_s , and the measured zero-crossing wave period, T_z , using the method given by SOULSBY (1987). Values for \hat{U}_w given by Eq. 7 and by the method of SOULSBY (1987) when compared with peak wave orbital velocities measured by the ECM pair positioned at $z \approx 30$ cm differed by less than 3% in all cases examined here.

Irrespective of bed morphology, the mobilisation, entrainment and resuspension of sand grains under moderate wave conditions is governed by the skin friction component of the total bed shear stress. For the rough turbulent wave boundary layer flows pertaining here, the skin friction factor for grain-scale roughness, f_{wG} , can be approximated using

$$f_{wG} = 0.237r^{-0.52} \quad (8)$$

(SOULSBY, 1997). Here the relative roughness, $r = A/k_{sG}$, the semi-orbital excursion $A = \hat{U}_w T/2\pi$, and the Nikuradse equivalent sand grain roughness $k_{sG} = \beta D_x$, where β is a constant and D_x refers to x percentile grain diameter. Whilst it is normally assumed that $k_{sG} = 2.5D_{50}$, values for βD_x given in the literature vary considerably from $1.25D_{35}$ to $5.1D_{84}$, SLEATH (1984, p. 39). This range of k_{sG} values may be attributed to factors such as the micromorphology of the bed, the flow regime adjacent to sediment grains and the motion of sediment grains on the bed at or close to threshold conditions. Estimates of f_{wG} are subject therefore to a certain degree of uncertainty, which is considered further in the following sections. Peak bed shear velocity values for grain-scale roughness, \hat{U}_{*wG} , were calculated using

$$\hat{U}_{*wG} = (0.5f_{wG}\hat{U}_w^2)^{0.5} \quad (9)$$

The ABP on STABLE provided *in situ* measurements of bed morphology from which estimates of the average ripple height, h_r , and wavelength, λ_r , were determined. However, in order to test here widely used formulae to predict the dimensions of wave-induced bed ripples, predictions of h_r and λ_r were also calculated using

$$\frac{h_r}{A} = 0.275 - 0.022\psi_w^{0.5} \quad \text{for } \psi_w < 156 \quad \text{and} \quad (10)$$

$$\frac{\lambda_r}{A} = 2.2 - 0.345\psi_w^{0.34} \quad (11)$$

for regular waves (NIELSEN, 1992). Here the sediment mobility number for waves, $\Psi_w = \hat{U}_w^2/(s-1)gD_{50}$, and the measured specific gravity of sediment grains, $s = 2.653$. For irregular wave conditions, h_r and λ_r values were calculated using

$$\frac{h_r}{A} = 21\psi_w^{-1.85} \quad \text{for } \psi_w > 10 \quad (12)$$

$$\frac{\lambda_r}{A} = \exp\left(\frac{693 - 0.37[\ln \psi_w]^8}{1000 + 0.75[\ln \psi_w]^7}\right) \quad (13)$$

(NIELSEN, 1992) where A is calculated using the significant wave height. Equation 12 and Eq. 13 were derived from field measurements. Further consideration is given below to measured and predicted vortex ripples and other bedforms measured during the experiment.

C-profiles

For a rippled bed in wave-only conditions, C-profiles can be described using the exponential convective model

$$C(z) = C_0 e^{-z/L} \quad (14)$$

(NIELSEN, 1992) where the vertical length-scale, L , parameterising the vortex ejection process in oscillatory flow over ripples is defined as

$$L = 0.075 \frac{\hat{U}_w}{w_s} h_r \quad \text{for } \frac{\hat{U}_w}{w_s} < 18 \quad (15)$$

$$L = 1.4h_r \quad \text{for } \frac{\hat{U}_w}{w_s} \geq 18 \quad (16)$$

NIELSEN (1992). $C(z)$ is the time-averaged suspended sediment concentration value at height z and C_0 is the so-called 'reference concentration' of suspended sediment at the bed ($z = 0$) defined as

$$C_0 = 0.005\Xi^3 \quad (17)$$

(NIELSEN, 1992). Values for Ξ were calculated using

$$\Xi = \frac{\rho(f_{wR})\hat{U}_w^2}{2(\rho_s - \rho)gD_{50}(1 - \pi h_r/\lambda_r)^2} \quad (18)$$

where f_{wR} is a rough bed wave friction factor calculated using Eq. 8. Here, the ripple-scale roughness, k_{sR} , defined approximately as $8h_r^2/\lambda_r$ (NIELSEN, 1992), was used to calculate r (Eq. 8).

For combined wave-current conditions in the field and in the laboratory has been shown that measured C-profiles can be simulated accurately using a diffusion-base expression in the form

$$C(z) = C(a) \left(\frac{z + L\alpha}{a + L\alpha} \right)^{-\alpha} \quad (19)$$

WILLIAMS *et al.* (1997b; 1998a). In Eq. 19, $C(a)$ is the time-averaged suspended sediment concentration value at height a . In the present wave-only conditions, the term parameterising average bed shear velocity in combined wave-current conditions is omitted so that the Rouse-type coefficient α parameterising diffusive processes is defined here as $w_s/\gamma\kappa \hat{U}_{*wG}$.

Here in accord with convention it is assumed that the ration of sediment diffusivity to eddy viscosity $\gamma = 1.0$ and the von Kármán constant, $\kappa = 0.4$. In common with Eq. 14, L is defined by bedform morphology and is used here to parameterise the vortex ejection mechanism (Eqs. 15 and 16).

$C(a)$ values in Eq. 19 were estimated using two existing expressions. In the first case, $C(a)$ values at $z = 2D_{50}$ were calculated using the ZYSERMAN and FREDSE (1994) expression

$$C(a) = \frac{0.331(\theta_s - 0.045)^{1.75}}{1 + 0.72(\theta_s - 0.045)^{1.75}} \quad (20)$$

for steady flow conditions. Here the skin friction Shield parameter, θ_s , is defined as $\hat{\tau}_{wG}/\rho(s - 1)gD_{50}$. In the second case, $C(a)$ values at $z(a) = h_r$ were calculated using the VAN RIJN (1984) expression

$$C(a) = \frac{0.015D_{50}T_*^{1.5}}{z(a)D_*^{0.3}} \quad (21)$$

In this case, the dimensionless grain size, D_* was calculated using $D_{50S} = D_{50}$ (Eq. 4). In the VAN RIJN formulation, the transport stage parameter, T_* , is defined as $(\hat{\tau}_{wG} - \tau_c)/\tau_c$, where $\hat{\tau}_{wG}$ is the peak wave induced bed shear stress for grain-scale roughness (*i.e.*, $\rho\hat{U}_{*wG}^2$).

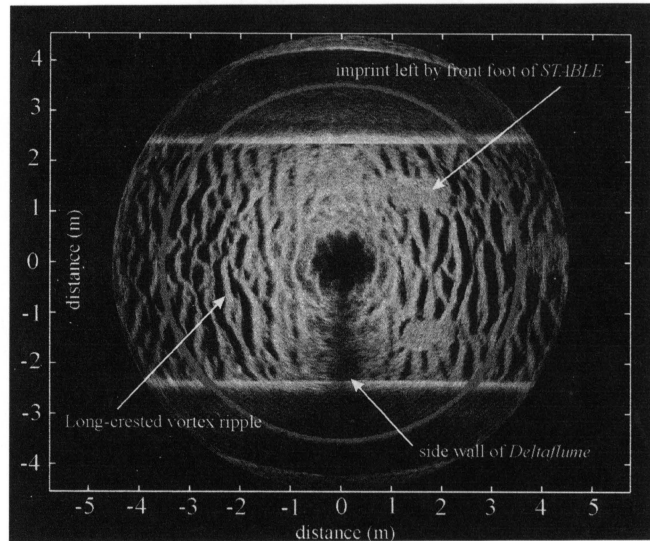
RESULTS AND DISCUSSION

Measured and Predicted Bedforms

Ripple height, h_r , is an important parameter in determining vortex entrainment of sediment by waves, and acts to define a mixing length in convective expressions for the prediction of C -profiles. Thus, attention is first turned to bed morphology measured by the ABP during the experiments. Tests on the medium sand bed produced ripples with wavelengths ≈ 0.3 m and heights ≈ 0.06 m. Tests on the fine sand bed in wave conditions where H or $H_s < 0.75$ m gave ripples with wavelengths ≈ 0.2 m and heights ≈ 0.03 m. Typically, during a 20-minute test, slightly asymmetric wave-induced flows and a weak near-bed return flow ≈ 0.01 m/s in the Deltaflume caused these ripples migrated a distance of approximately 0.05 m toward the wave generator. In addition to the vortex ripples measured during lower wave conditions, the fine sand bed showed a tendency to develop much larger, 'dune-like' bedforms ($h_r \approx 0.15$ m, $\lambda_r \approx 2.0$ m) under larger wave conditions.

Plan view images of vortex ripples on the medium and the fine sand bed obtained using the SSS instrument are shown in Figure 2. In Figure 2a, the image was obtained in front of STABLE following test A12a, and shows clearly imprints left by the feet following removal of the rig from the Deltaflume. In Figure 2b, the image was obtained from a position behind STABLE following test f08a when the rig was still in the flume. In this case, STABLE feet are shown to be elevated above the general level of the bed and an acoustic shadow from the rear leg of STABLE is evident. Figure 2a shows that ripples are long-crested and approximately 2-dimensional and that visually, ripples appear to be similar in front of and beneath STABLE. Whilst ripples shown in Figure 2b are

(a) medium sand bed (ripple troughs shown shaded black)



(b) fine sand bed (ripple troughs shaded black)

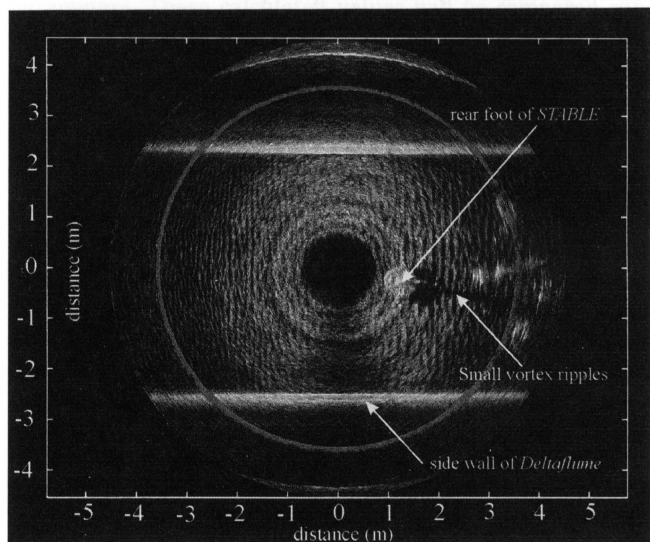


Figure 2. Sector scanning sonar images of ripples on (a) the medium sand bed and (b) the fine sand bed, showing the side-walls of the Deltaflume and the location of STABLE. Visual differences between ripples beneath STABLE and at distances away from the rig are not discernible.

much smaller in both amplitude and wavelength than the ripples on the medium sand bed, they to also appear to be long crested and two-dimensional.

In the following discussion of bed profiles measured using the ABP, 'instantaneous' bed profiles refer to profiles measured during a test every 30 seconds, and 'time-average' bed profiles refer to the mean bed elevation during the 20 minute measurement period at each ABP measurement cell along the bed transect. Figure 3a shows time-averaged bed profiles for all the tests considered here. Estimates for h_r and λ_r used

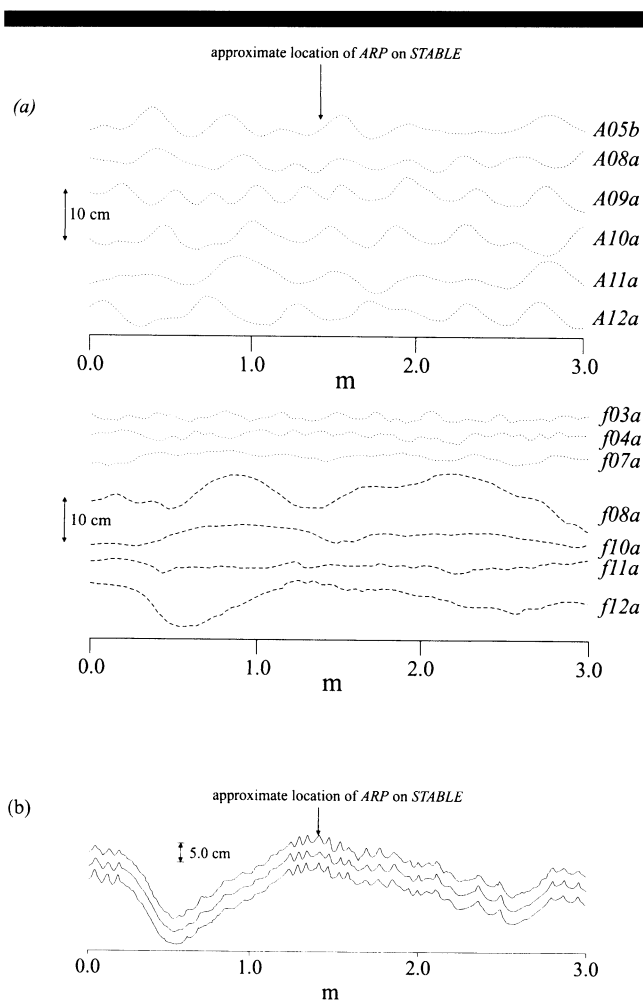


Figure 3. (a) Time-averaged bed profiles measured using the ABP along a 3.0 m transect for tests on the medium and fine sand beds; (b) instantaneous bed profiles measured using the ABP on a bed of fine sand during large waves showing 'dunes' and small 'vortex' ripples.

below were obtained using the time-averaged bed morphology data.

Whilst vortex ripples and the dune-like bedforms present on the fine sand bed in high wave conditions could be readily identified in the majority of tests, it was not possible to detect small ripple in average bed profiles for tests f08a, f10a, f11a and f12a (Figure 3a). However, examination of the instantaneous bed profiles measured during these tests revealed small ripples with $\lambda_r \approx 0.1$ m and $h_r \approx 0.02$ m to be present of along the crest region of the larger bedforms. Measurement showed that these small ripples migrated at a much quicker rate than those present in the lower wave conditions (≈ 0.1 m) and consequently they were not detected in the time-averaged profiles. Figure 3b shows the small vortex ripples present with the larger dune-like bedforms on three individual instantaneous bed profiles measured during test f12a. It is the dimensions of these smaller ripples that will be used below to calculate the mixing term L used in Eq. 14 and Eq. 19 for tests f08a, f10a, f11a and f12a.

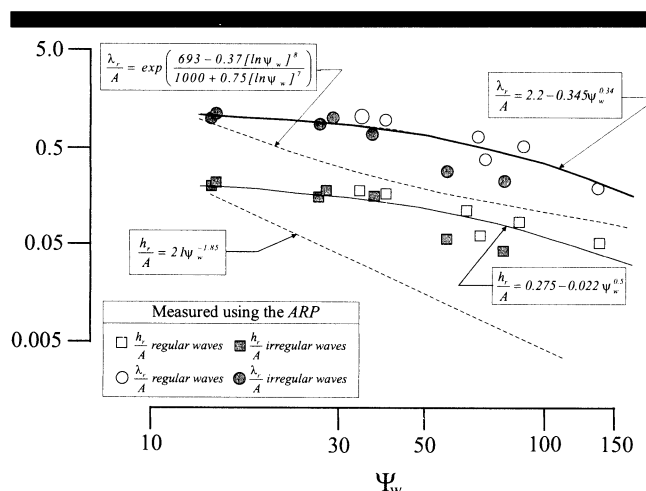


Figure 4. Comparison between relative ripple height, h_r/A , and relative wavelength, λ_r/A , values measured by the ABP and values predicted by various empirical formulae (NIELSEN, 1992).

The relationship between measured h_r/A , λ_r/A and Ψ_w for the medium and the fine sand beds is shown in Figure 4. This figure also shows values for h_r/A and λ_r/A predicted for regular waves in the laboratory (Eq. 10 & Eq. 11, respectively) and for irregular waves in the field (Eq. 12 & Eq. 13, respectively) (NIELSEN, 1992). Over the range $10 < \Psi_w < 150$, Figure 4 shows generally good agreement between h_r/A and λ_r/A values measured by the ABP and h_r/A , and λ_r/A values predicted by Eq. 10 and Eq. 11 for regular wave conditions. The three exceptions to this are during tests f10a, f11a and f12a, when smaller than expected ripples ($h_r \approx 0.02$ m; $\lambda_r \approx 0.1$ m) were present with the dune-like bedforms not predicted by theory (Figure 3). Images of the bed obtained using the SSS showed these large bedforms to be present both in the vicinity of the STABLE frame and at locations up to 5m away from the frame. It is considered therefore, that these large bedforms are not simply the result of complex interactions between wave-induced flow and STABLE. These large bedforms were absent during all tests over the medium sand bed. Values for h_r/A and λ_r/A predicted by Eq. 12 and Eq. 13 for random wave conditions differ markedly from the measured values. Similar findings are reported by RIBBERINK and AL-SALEM (1994). It is considered that in the present cases, insufficient time elapsed during the random wave runs for the bed morphology to evolve to an equilibrium form.

Calculated and Measured Sediment and Hydrodynamic Parameters

In the following sections we present ourselves initially with a situation frequently encountered when attempting to predict sediment transport for scientific and engineering applications in the field: namely measurements of only a few basic sedimentological and hydrodynamic parameters. Thus, with the exception of data for grain size and density, wave height and period and water depth, all the terms required to predict C-profiles using Eq. 14 and Eq. 19 were calculated using the

equations described above. A rigorous test of the models is then to compare predicted C-profiles with C-profiles measured during the experiments. Fine tuning of parameters required to achieve closer agreement between measured and predicted C-profiles may then aid further our understanding of the processes resulting in suspended sediments under waves. A summary of the principal sediment and hydrodynamic parameters necessary to predict C-profiles for the present series of tests is given in Table 2. Table 2 also includes the following measured and calculated wave and sediment parameters: H ; H_s ; T ; T_p ; T_z ; h_r and λ_r .

Table 3 shows D_{50S} values predicted by Eq. 1 and D_{50S} values measured by sieve analysis of the pump-samples obtained from STABLE at the stated heights above the bed. In nearly all cases measured D_{50S} values are $\approx 10\%$ less than D_{50S} values predicted by the VAN RIJN (1984) formula. However, since the range of heights over which Eq. 1 is valid is not defined, the significance of this difference cannot be quantified. In common with findings reported by WHITEHOUSE (1995) for tidal flows, measured D_{50S} values over the range $5.3 \text{ cm} < z < 40 \text{ cm}$ equate approximately with D_{16} – D_{35} values for the sediments comprising the bed (Figure 1c). Table 3 shows that measured D_{50S} values decrease with distance above the bed to values approximately equal to D_{10} for the bed sediment at $z = 40 \text{ cm}$. A reduction in the diameter of grains in suspension of approximately 0.07 mm was typically measured over the range $5.3 \text{ cm} < z < 40.0 \text{ cm}$. Differences between D_{50S} values measured from the side-wall of the Deltaflume and those given in Table 3 were small and showed no systematic trend. Given that differences between measured and predicted D_{50S} values are small and the lack of data from position at $z < 5.3 \text{ cm}$, it was decided to proceed with the D_{50S} values predicted by Eq. 1. This is consistent with the present requirement to use calculated parameters as far as possible.

Measured C-profiles

C-profiles measured using the pump-sampling equipment on STABLE are shown in Figure 5 for: (a) regular waves above the medium and fine sand beds [(i) tests A05b, A08a, A11a, and (ii) f03a, f08a, f11a, respectively]; and (b) for irregular waves above the medium and fine sand beds [(i) tests A09a, A10a, A12a, and (ii) f04a, f07a, f12a, respectively]. Figure 5 shows also C-profiles measured during the same test conditions from the side wall of the Deltaflume. For the C-profiles considered here, time-averaged suspended sediment concentration, \bar{C} , values measured at the sampling position closest to the bed span a range from approximately 0.01 g/l to 10.0 g/l . Whilst Figure 5 shows that the majority of C-profiles exhibit a slightly convex curvature, there are some examples (e.g., f04a) where ‘S’-shaped profiles are evident and others where profiles are approximately linear (e.g., A10a).

Figure 6 shows comparisons between measured C-profiles and C-profiles calculated using Eq. 14 and Eq. 19. Values of the parameters $C(a)$, L , \hat{U}_w , w_s , \hat{U}_{*wG} , τ_T used in Eq. 14 and Eq. 19 were calculated using the methods described above and are given in Table 2.

In using Eqs. 14 and 19, selection of appropriate parame-

Table 2. Measured and calculated sediment and hydrodynamic parameters used in modelling \bar{C} profiles for tests on the medium sand bed ($\sigma_s = 1.7$; $\tau_i = 0.20 \text{ N/m}^2$; $w_s = 0.031 \text{ m/s}$) and on the fine sand bed ($\sigma_s = 1.56$; $\tau_i = 0.15 \text{ N/m}^2$; $w_s = 0.013 \text{ m/s}$).

Parameter	Units	A08a	A05b	A11a	A12a	A09a	A10a	f03a	f08a	f11a	f04a	f07a	f10a	f12a
H	m	0.81	1.09	1.23	1.22	0.79	1.01	0.54	1.07	0.76	0.54	0.78	1.04	1.37
H_s	m	5.0	5.0	5.0	5.1	4.9	5.1	5.0	5.0	5.0	4.9	4.8	5.3	4.5
T	s				4.0	3.8	4.0				3.9	3.7	4.1	3.5
T_p	s				1.23	1.27	1.23				1.27	1.33	1.19	1.39
T_z	s				0.44	0.28	0.38				0.19	0.27	0.39	0.45
ω	s^{-1}	1.25	1.25	1.25	0.36	0.22	0.31	1.25	1.25	1.25	0.15	0.20	0.32	0.33
U_w	m/s	0.45	0.60	0.69	0.36	0.22	0.31	0.30	0.60	0.42	0.15	0.20	0.32	0.33
A	m	0.36	0.48	0.55	0.36	0.22	0.31	0.24	0.47	0.34	0.05	0.02	0.33	0.33
T_s	—	0.65	0.80	1.12	0.58	0.41	0.58	0.20	1.32	0.54	0.05	0.02	0.33	0.33
D_s	—	6.30	6.31	6.33	6.30	6.28	6.29	3.23	3.26	3.24	3.23	3.23	3.24	3.25
D_{50}	—	0.060	0.051	0.048	0.056	0.048	0.055	0.040	0.015	0.020	0.030	0.036	0.020	0.020
h_r	m	0.35	0.31	0.29	0.32	0.24	0.30	0.24	0.08	0.11	0.15	0.22	0.11	0.11
λ_r	m	3.3	1.7	1.6	3.2	0.9	3.9	1.9	0.9	1.1	5.2	1.8	1.2	1.1
$k_{wG} \times 10^{-4}$	m	10871	2817	3406	1234	229	789	1247	4876	3100	292	1127	2683	2954
$k_{wR} \times 10^{-2}$	m	8.3	6.7	6.3	7.9	7.8	7.9	5.3	2.3	2.9	4.8	4.8	3.0	2.9
$f_{wG} \times 10^{-3}$	—	6.2	3.8	3.4	6.0	14.0	7.4	5.8	2.9	3.9	12.3	6.1	3.9	3.7
$f_{wR} \times 10^{-2}$	—	12.7	8.9	7.8	12.3	17.9	13.7	12.4	4.6	6.4	16.1	12.9	6.8	6.6
$U_{*wG} \times 10^{-2}$	m/s	2.5	2.6	2.9	2.5	2.3	2.3	1.6	2.2	1.8	1.5	1.5	1.7	1.0
$L \times 10^{-2}$	m	5.5	7.1	6.7	5.1	2.8	4.3	5.6	2.1	2.8	3.4	5.0	2.8	2.9
Ψ_w	—	38	68	88	37	15	27	34	135	70	14	28	57	78

Table 3. Median suspended sediment grain size, D_{50s} , for medium and fine sand predicted using Eq. 1 and measured using pump-samples from STABLE.

Test	D_{50s} (m) (VAN RIJN, 1984)	D_{50s} (mm) ($z = 5.3$ cm)	D_{50s} (mm) ($z = 7.3$ cm)	D_{50s} (mm) ($z = 10.2$ cm)	D_{50s} (mm) ($z = 25.5$ cm)	D_{50s} (mm) ($z = 40.0$ cm)
A05b	0.27					
A08a	0.27	0.26	0.23	0.22	0.19	0.18
A09a	0.27	0.27	0.24	0.23	0.21	
A10a	0.27		0.23	0.22	0.19	
A11a	0.27	0.24	0.22	0.21	0.18	0.15
A12a	0.27					
f03a	0.14	0.13	0.11	0.10	0.09	0.09
f04a	0.14	0.12	0.11	0.10		
f07a	0.14	0.12	0.11	0.10	0.10	0.09
f08a	0.14		0.12	0.11	0.09	0.09
f10a	0.14		0.13	0.11	0.09	0.09
f11a	0.14					
f12a	0.14		0.14	0.13	0.11	0.10

terisation for k_{sG} (Eq. 8) was at first problematic. For example, use of $5.1D_{84}$ (MAHMOOD, 1971) in the expression to calculate r gave markedly different results to values obtained using $1.25D_{35}$ (ACKERS and WHITE, 1973) to parameterise grain roughness. This in turn influenced significantly the value of \hat{U}_{*wG} and hence affected values of $C(a)$ obtained using Eqs. 20 and 21. The approach adopted here was to assume $D_x = D_{50}$ and to optimise the fit between predicted and measured \bar{C} values at $z = 5.3$ cm by varying β . Following this procedure gave good agreement between measured C-profiles and C-profiles predicted by Eq. 19, Figure 6. Here we choose to calculate the reference concentration using Eq. 20. In contrast, C-profiles predicted by Eq. 14 (using Eqs. 15 or 16 to calculate the empirical coefficient L) follow approximately the same shape as those predicted by Eq. 19 over the range $2.5D_{50} < z < 3$ cm but deviate significantly from measured C-profiles at $z > 5$ cm. These results contrast with the good agreement found between C-profiles measured in the field by LEE and HANES (1996) and the convective model of NIELSEN (1992), Eq. 14.

Since the grain roughness parameter k_{sG} must be related to the size and arrangement of grains on the bed, it might be anticipated that β is related to the sediment mobility number Ψ_w if, for example, D_{50} is selected as being a characteristic length scale describing grains comprising the bed. The relationship between β and Ψ_w for $D_x = D_{50}$ suggested by the model (Figure 7) demonstrates that the grain roughness decreases with Ψ_w over the range $10 < \Psi_w < 100$. For $\Psi_w > 100$, a single data value from the present tests suggests that β values may begin again to increase. For $D_x = D_{50}$, the relationship between β and Ψ_w can be described using

$$\ln(\beta) = 8.5 - 3.8 \ln(\Psi_w) + 0.4 \ln(\Psi_w)^2 \quad (22)$$

Whilst it is well known that k_{sG} values are much larger in sheet flow conditions (*i.e.*, $\Psi_w > 150$), *e.g.*, WILSON (1989), systematic changes in the hydraulic roughness of beds subject to sporadic or periodic mobility have not been reported. Thus, with knowledge of the mobility number, Figure 7 indicates a method by which k_{sG} can now be defined over a range of hydrodynamic conditions. Further, as many combinations of grain size parameters and multipliers can give the same k_{sG} value, the relationship shown in Figure 7 may also

explain the wide range of definitions for k_{sG} reported in the literature (*e.g.*, SLEATH, 1984). It should be noted also that β values are derived here using an empirical fit to laboratory data, and thus it is possible that changes in β simply reflect a shortcoming of Eq. 19. Further work to investigate this will be the subject of a future publication by the authors.

Values for the sediment diffusivity, ϵ_w , were calculated for C-profiles measured from STABLE and from the Deltaflume using the expression

$$\epsilon_w = \frac{-w_s \bar{C}}{\partial \bar{C} / \partial z} \quad (23)$$

derived from the familiar time-averaged and horizontally spatially averaged sediment continuity equation. Similarly, ϵ_w values were also calculated for C-profiles predicted by Eq. 19. In all cases, ϵ_w values were found to increase linearly with z and exhibited relatively little scatter adding further to confidence in the accuracy of the present \bar{C} measurements. Using least-squares linear regression analysis of ϵ_w on z , values for the total diffusive bed shear velocity, U_{*total} , were obtained from the gradient. In all cases, the correlation was found to be statistically significant at the 99% confidence level. Values for a constant wave mixing coefficient, $\bar{\epsilon}_w$, parameterising the vortex-ejection mechanism over ripples were obtained from the intercept with the abscissa (*cf.* WILLIAMS *et al.*, 1998a).

Values for U_{*total} obtained from the measured and predicted C-profiles are plotted against \hat{U}_{*wG} values from Eq. 9 in Figure 8. Values for U_{*total} from the predicted C-profiles (Eq. 19) lie on the unity line approximately mid-way between the measured U_{*total} values which themselves exhibit relatively little scatter. These data provide further evidence that diffusive processes are correctly parameterised in Eq. 19.

A wave-mixing coefficient can be extracted from the empirical length scales given by NIELSEN (1992) for suspended sediment concentrations in oscillatory-only flow over ripples composed of fine sand grains from $\bar{\epsilon}_w = Lw_s$. For $A\omega/w_s < 18$, $\bar{\epsilon}_w = 0.075 A\omega h_r$, and for $A\omega/w_s \geq 18$, $\bar{\epsilon}_w = 1.4h_r$ (NIELSEN, 1992). Here ω is the angular wave velocity = $2\pi/T$. Figure 9 shows good agreement between $\bar{\epsilon}_w$ values predicted by the model and $\bar{\epsilon}_w$ values derived from the measured C-profiles. In addition, Figure 9 also shows the $\bar{\epsilon}_w$ values predicted using the Nielsen empirical formulae agree closely with measured

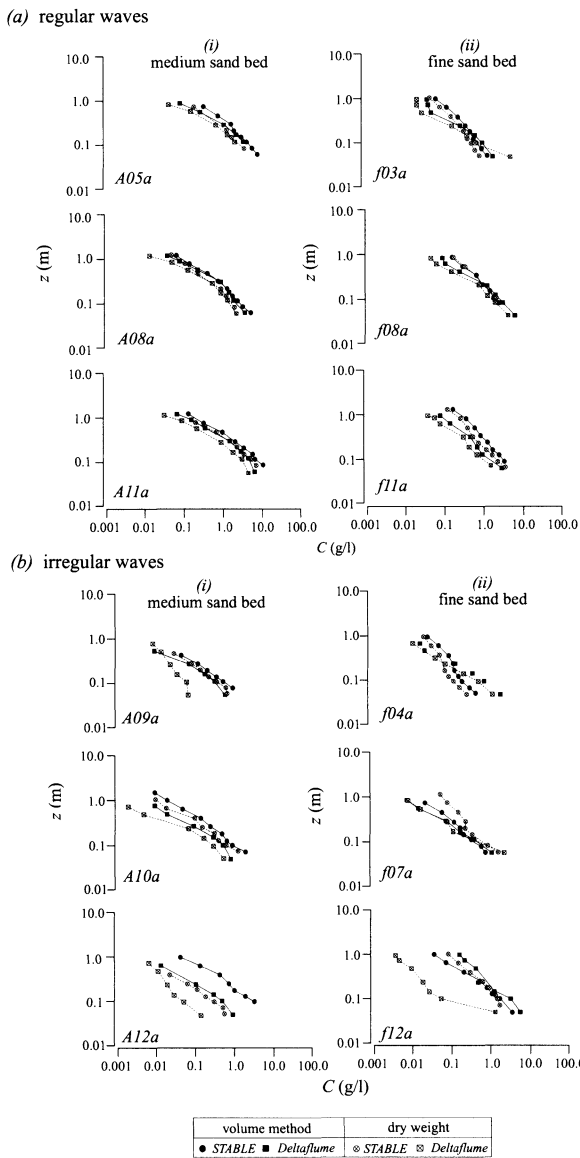


Figure 5. C-profiles measured in regular and irregular wave conditions above rippled beds of medium and fine sand using pump-sampling from STABLE and from the Deltaflume.

values. Figure 9 thus demonstrates that values of L used in Eq. 19 parameterise well convective processes leading to the resuspension of sand.

SUMMARY AND CONCLUSIONS

Experiments to study sediment resuspension at approximately field-scale have been undertaken in the Deltaflume. Field and laboratory instruments have been used to measure sediment properties, hydrodynamic conditions and C-profiles. Valuable data from the present experiments are presented pertaining to bedforms and suspended sediment concentration profiles. Published methods have been used to calculate all the terms used to predict C-profiles using a convective

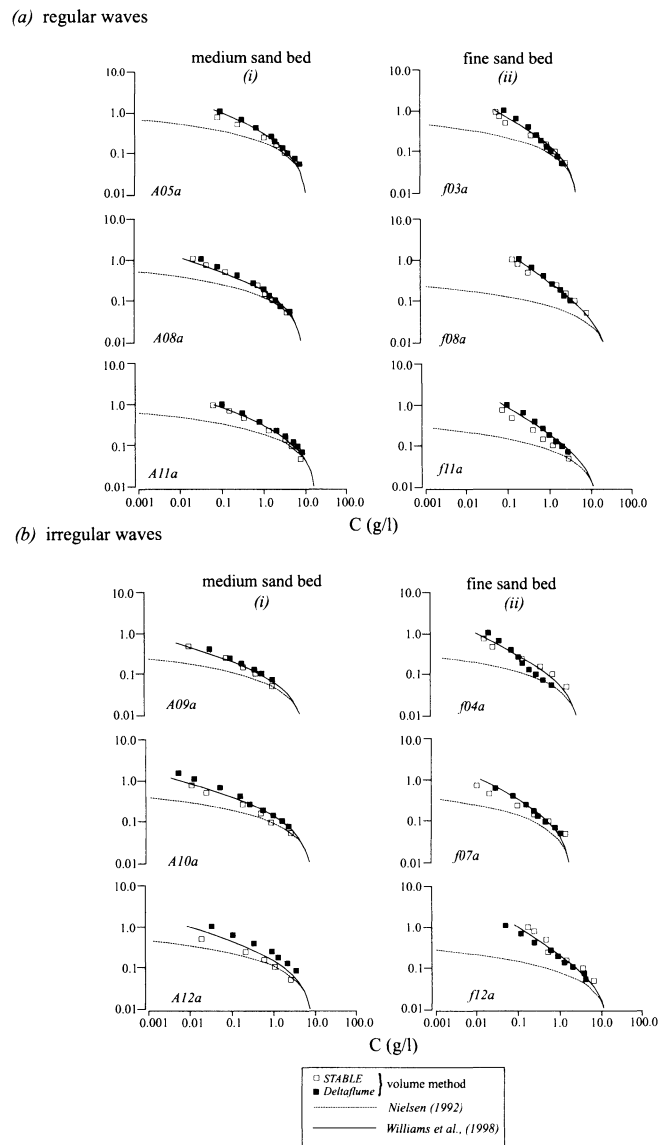


Figure 6. Measured (Deltaflume and STABLE) and predicted (NIELSEN, 1992; WILLIAMS *et al.*, 1997b) C-profiles for regular and irregular waves above the rippled medium and the fine sand beds.

model and new model using a diffusion-based formulation. It was found that at all elevations, D_{50S} values measured by sieving were $\approx 10\%$ smaller than predicted D_{50S} values. Settling velocity values may be slightly overestimated therefore, if predicted D_{50S} values are used. Whilst at $z = 5.3$ cm, D_{50S} values $\approx D_{35}$ for sediment comprising the bed, at elevations > 7.3 cm, D_{50S} values equated more closely with D_{16} . In the expression $k_{sG} = \beta D_x$ for grain-scale bed roughness it has been shown that for the present experimental conditions, β is a non-linear function of the wave mobility number, Ψ_w when $D_x = D_{50}$. It has been observed that over the range $10 < \Psi_w < 100$, β decreases, whilst for $\Psi_w > 130$, β increases. It is considered that whilst these results go some way in rec-

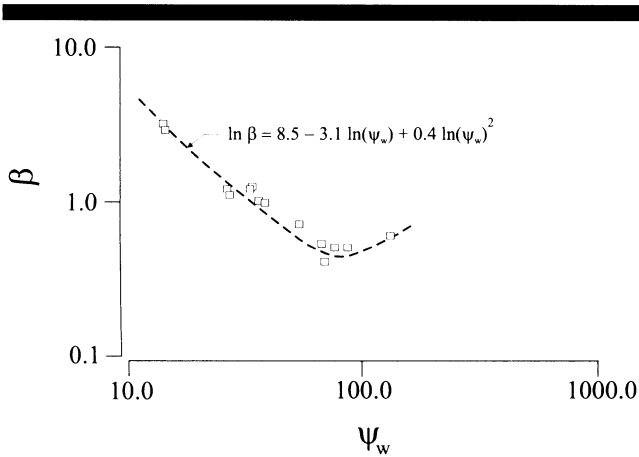


Figure 7. Relationship between β and sediment mobility number, Ψ_w , assuming $D_x = D_{50}$.

onciling the wide variation in terms used to define k_{sG} , they may also point to some deficiencies in various approaches for the scaling of grain-related bed roughness. A new model has been used to predict accurately measured C-profiles in a wide range of wave conditions for both medium and fine sands. The expression is relatively simple to apply and through use of well-known sediment and hydrodynamic equations, requires only a few simple input parameters. In agreement with theory a statistically significant positive linear correlation was found between ϵ_w values and z. Good agreement between $\bar{\epsilon}_w$ values predicted by the model and $\bar{\epsilon}_w$ values from the measured C-profiles demonstrates that values of L used here parameterise well bedform morphology and associated scales of the convective processes leading to the resuspension of sand.

ACKNOWLEDGEMENTS

The work was jointly supported by the European Communities through the TMR Programme "Access to Large Scale

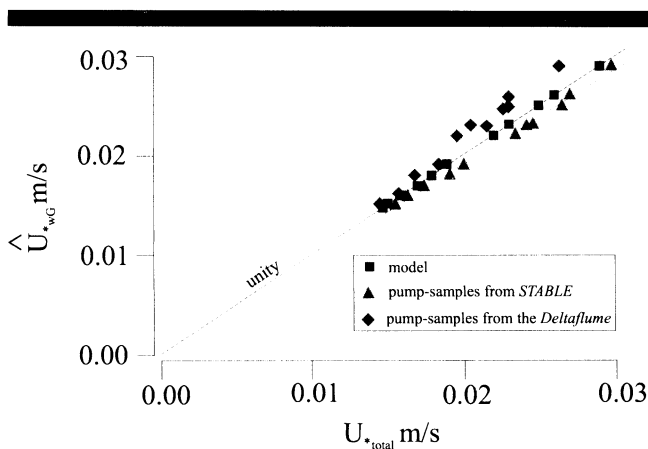


Figure 8. Measured and computed values for sediment diffusivity, U_{*sed} , for tests on the medium and the fine sand beds.

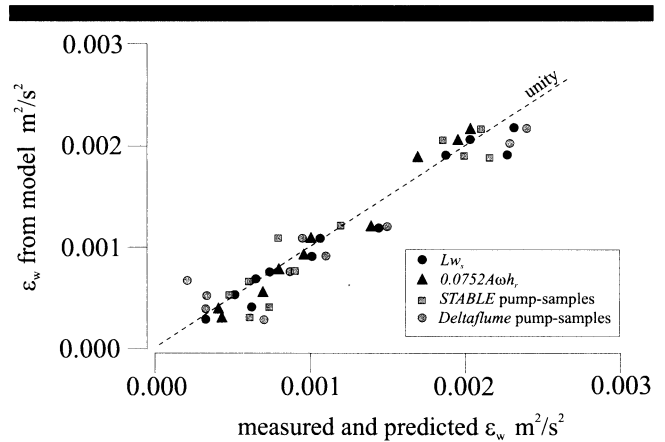


Figure 9. Measured and predicted (NIELSEN, 1992) values for the wave mixing coefficient, $\bar{\epsilon}_w$.

Facilities", the MAST 3 project 'Inlet Dynamics Initiative: Algarve' (INDIA) contract MAS3-CT97-0106; the UK NERC; and The Flood and Coastal Defence Division of MAFF, UK.

LITERATURE CITED

ACKERS P. and WHITE W., 1973. Sediment transport: a new approach and analysis. *Journal Hydraulic Division ASCE*, 99, 2041-2060.

BELL P.S. and THORNE P.D., 1997. Measurements of sea bed ripple evolution in an estuarine environment using a high resolution acoustic sand ripple profiling system. *Proceedings Oceans'97 Conference*, 6-9 October, Halifax, Nova Scotia, Volume 1. MTS/IEEE, Washington D.C., pp. 339-343.

BELL P.S.; THORNE P.D., and WILLIAMS J.J., 1998. Acoustic measurements of sand ripple profile evolution under controlled wave conditions. *4th International Conference on Underwater Acoustics* (Rome), pp. 353-358.

BOSMAN, J.J.; VELDEN, E.T.; VAN DER, J.M., and HULSBERGEN C.H., 1987. Sediment concentration measurements by transverse suction. *Coastal Engineering*, 11, 353-370.

HAVINGA, F.J., 1992. Sediment concentrations and sediment transport in case of irregular non-breaking waves with a current. *Report H840 Parts E, F & G, Delft Hydraulics*, Delft University of Technology, Delft, The Netherlands.

HUMPHERY J.D. and MOORES S.P., 1994. STABLE II - An improved benthic lander for the study of turbulent wave-current-bed interactions and associated sediment transport. *Electronic Engineering in Oceanography, IEE Conference Publication No. 394*, pp. 170-174.

JONSSON, I.G., 1966. Wave boundary-layers and friction factors. *Proceedings of the 10th Conference on Coastal Engineering* (Tokyo, Japan), pp. 127-148.

LEE T.H. and HANES D.M., 1996. Comparison of field observations of the vertical distribution of suspended sand and its prediction by models. *Journal of Geophysical Research*, 101(C2), 3561-3572.

MAHMOOD K., 1971. Water Management Technical Report 11. *Colorado State University*, Fort Collins, Colorado, USA, 50p.

NIELSEN, P., 1992. *Coastal Bottom Boundary Layer and Sediment Transport*. World River Edge, N.J.: Scientific Publishing 324p.

RIBBERINK J.S. and AL-SALEM A.A., 1994. Sediment transport in oscillatory boundary layers in cases of rippled beds and sheet flow. *Journal of Geophysical Research*, 99(C6), 12707-12727.

SLEATH, J.F.A., 1984. *Sea Bed Mechanics*. New York: Wiley 335p.

SLEATH, J.F.A., 1991. Velocities and shear stresses in wave-current flows. *Journal of Geophysical Research*, 96, C8, 15237-15244.

- SOULSBY, R.L., 1987. Calculating bottom orbital velocity beneath waves. *Coastal Engineering*, 11, 371–380.
- SOULSBY, R.L., 1997. *Dynamics of Marine Sands: a Manual for Practical Applications*. HR Wallingford Report SR466, 142p.
- VAN RIJN, L.C., 1984. Sediment transport Part I: bed load transport; part II: suspended load transport; and part III: bed forms and alluvial roughness. *Journal of the Hydraulics Division ASCE*, 110, HY10, 1431–1456; HY11, 1613–1641; HY12, 1733–1754.
- WHITEHOUSE R.J.S., 1995. Observations of the boundary layer characteristics and the suspension of sand at a tidal site. *Continental Shelf Research*, 15, 1549–1567.
- WILLIAMS, J.J.; BELL, P.S.; COATES, L.E.; HARDCASTLE, P.J.; HUMPHERY, J.D.; MOORES, S.P.; THORNE, P.D., and TROUW K., 1997a. Evaluation of field equipment used in studies of sediment dynamics. *Proudman Oceanographic Report*, 5/3, 45p. (unpublished manuscript).
- WILLIAMS, J.J.; ROSE, C.P.; THORNE, P.D.; COATES, L.E.; WEST, J.R.; HARDCASTLE, P.J.; HUMPHERY, J.D.; MOORES, S.P., and WILSON, D.J., 1997b. Observed suspended sediments in storm conditions. *Proceedings ICCE'96 (ASCE)*, 3, 3257–3269.
- WILLIAMS, J.J.; ROSE, C.P.; THORNE, P.D.; O'CONNOR, B.A.; HUMPHERY, J.D.; HARDCASTLE, P.J.; MOORES, S.P.; COOKE, J.A., and WILSON, D.J., 1998a. Field observations and predictions of bed shear stresses and vertical suspended sediment concentration profiles in wave-current conditions. *Continental Shelf Research*, 19, 507–536.
- WILLIAMS, J.J.; BELL, P.S.; COATES, L.E.; DAVIES A.E.; HARDCASTLE, P.J.; HUMPHERY, J.D.; MOORES, S.P.; VAN RIJN L.C.; THORNE, P.D., and TROUW K., 1998b. Laboratory evaluation of instrumentation used in field studies of wave-sediment interactions. *Proceedings ICCE'98 (ASCE)*, 3, 2423–2434.
- WILSON K.C., 1989. Mobile bed friction at high shear stress. *J. Hydraulic Engineering, ASCE*, 115, 825–830.
- ZYSERMAN, J.A. and FREDSSØE, J., 1994. Data analysis of bed concentration of sediment. *Journal of Hydraulic Engineering*, 120 (9), 1021–1042.

APPENDIX 1 NOMENCLATURE

- | | | | |
|-----------|--|--------------------|--|
| A | = semi-orbital wave excursion | D_{90} | = 90% of grains finer than stated value |
| \bar{C} | = time-averaged suspended sediment concentration | D_x | = x% of grains finer than stated value |
| C(a) | = time-averaged 'reference' suspended sediment concentration at height z = a | H | = wave height (monochromatic waves) |
| C(0) | = time-averaged 'reference' suspended sediment concentration at height z = 0 | H_s | = significant wave height |
| C(z) | = time-averaged 'reference' suspended sediment concentration at height z | L | = vertical length scale (NIELSEN, 1992) |
| D_* | = dimensionless grain size | T | = wave period (monochromatic waves) |
| D_{*s} | = dimensionless grain size for particles in suspension | T_p | = peak wave period |
| D_{10} | = 10% of grains finer than stated value | T_s | = sediment transport parameter |
| D_{16} | = 16% of grains finer than stated value | T_z | = zero-crossing wave period |
| D_{35} | = 35% of grains finer than stated value | T_* | = transport stage parameter |
| D_{50} | = 50% of grains finer than stated value | \hat{U}_w | = peak wave orbital velocity |
| D_{50S} | = median diameter of grains in suspension | \hat{U}_{*wG} | = peak wave-only bed shear velocity for grain-scale roughness |
| D_{84} | = 84% of grains finer than stated value | \hat{U}_{*wR} | = peak wave-only bed shear velocity for ripple-scale roughness |
| | | U_{*total} | = total diffusive bed shear stress |
| | | f_{wG} | = wave friction factor for grain-scale roughness |
| | | f_{wR} | = wave friction factor for ripple-scale roughness |
| | | g | = acceleration due to gravity |
| | | h | = water depth |
| | | h_r | = ripple height |
| | | k | = wavenumber |
| | | k_{sG} | = Nikuradse equivalent sand grain roughness |
| | | r | = relative roughness (A/K_s) |
| | | s | = specific gravity of sediment |
| | | W_s | = settling velocity for sediment grains |
| | | x | = distance across the Deltaflume |
| | | y | = distance along the Deltaflume |
| | | z | = height above the sediment bed |
| | | α | = Rouse-type parameter |
| | | β | = multiplier |
| | | ϵ_w | = sediment diffusivity |
| | | $\bar{\epsilon}_w$ | = wave mixing coefficient |
| | | λ | = wavelength of water waves |
| | | λ_r | = ripple wavelength |
| | | κ | = von Kármán's constant (0.4) |
| | | ν | = kinematic viscosity of water |
| | | θ_c | = critical Shields parameter |
| | | θ_s | = skin-friction wave-only Shields parameter |
| | | ρ | = density of water |
| | | ρ_s | = measured sediment density |
| | | σ_s | = grain sorting parameter |
| | | τ_τ | = threshold bed shear stress |
| | | $\hat{\tau}_w$ | = peak wave-only bed shear stress |
| | | $\hat{\tau}_{wG}$ | = peak wave-only bed shear stress for grain-scale roughness |
| | | Ξ | = rough bed Shields parameter |
| | | ω | = angular wave velocity |
| | | Ψ_w | = sediment mobility number for waves |